Enhancing mechanisms of arc-erosion resistance for copper tungsten electrical contact using reduced graphene oxides *in situ* modified by copper nanoparticles

LongLong Dong [a, b*], Liang Li [a], Xiang Li [a], Wei Zhang [a], YongQing Fu [c], Ahmed Elmarakbi [c], YuSheng Zhang [d]

[a] Advanced Materials Research Central, Northwest Institute for Nonferrous Metal Research, Xi'an, 710016, PR China

[b] School of Materials Science and Engineering, Northeastern University, Shenyang 110819, PR China

[c] Faculty of Engineering and Environment, Northumbria University, Newcastle upon Tyne NE1 8ST, UK

[d] Xi'an Rare Metal Materials Institute Co., Ltd, Xi'an, 710016, PR China

Abstract: To solve critical issues of premature failure for copper tungsten (CuW) based electrical contacts during arc erosion at the moment of arc breakdown, we proposed a new strategy of using metal doped reduced graphene oxides (rGOs) and *in-situ* formed tungsten carbides to inhibit movements of cathode spots during the arc ablation process.

* Corresponding author at: Advanced Materials Research Central, Northwest Institute for Nonferrous Metal Research, Xi'an 710016, PR China.
E-mail addresses: donglong1027@163.com (L.L. Dong)

CuW composites were reinforced with Cu modified rGO nanopowders (i.e. Cu@rGO) using combined processes of chemical co-reduction, ball milling and spark plasms sintering (SPS). Effects of Cu@rGO addition on microstructure, arc erosion resistance and arc ablation resistance of the CuW composites were systematically investigated. Results showed that tungsten carbides with irregular shapes were formed through *in-situ* reactions of rGO and tungsten during the SPS process. Arc erosion resistance of CuW composites was significantly improved owing to introduction of nanostructured Cu@rGO. Compared with those of CuW composites, the ablation areas of Cu@rGO/CuW ones were much smaller and the ablation craters were shallower, and the average strengths of dielectric vacuum breakdowns of the CuW composites with 3 wt% Cu@rGO were increased by 28.9%. The arc breakdown mechanisms of Cu@rGO/CuW composites were identified as: (1) The nanostructured Cu@rGO increases the viscosity of molten metal Cu, thus inhibiting its fast flow and splashing; (2) Lower work functions of carbon (i.e. rGO) and tungsten carbide restrain the electron emissions during arc breakdown; and (3) The tungsten carbides with their good stability and high melting point shorten the solidification time of molten copper liquid and extend the service life time of the Cu@rGO/CuW composites.

Keywords: Cu@rGO nanoparticles, microstructure, CuW composites, arc-erosion resistance

1. Introduction

Electrical contacts are key components used in high-voltage circuit-breaker, and are responsible for switching the currents on and off at super-high voltages. However, electric arc generated during contact and break operations inevitably destroys the electrode's surface under the combined actions of transient heat, mechanical impact and huge electromagnetic voltage. Therefore, performance and reliability of the contact materials will directly affect both life-time of switches and reliability of electrical operations [1-5]. It is crucial to ensure the contact materials with good thermal/electrical conductivities, high hardness, and high ablation resistance. Copper-tungsten (CuW) alloys have been explored for this application, which is benefited from the exceptional mechanical-physical properties of W skeleton (with its high hardness and high temperature strength, but a low thermal expansion coefficient) and excellent conductivity of Cu (with its good plasticity and thermal and electrical conductivities, but a high thermal expansion coefficient). CuW is often regarded as a typical pseudo-alloy without mutual miscibility or reactions between W and Cu [6-7].

Recently, there are increased requests for the CuW alloys to be applied as high power/voltage electrical contacts under severe service conditions. Therefore, it is critical to improve the contact materials' mechanical properties and arc ablation resistance. Two main approaches have often been adopted for this purpose. The first one is to refine grains of W matrix [8-10]. Frequently nano-sized W powders were chosen as the raw material, however, this often results in their severe agglomeration during blending/mixing process. The second commonly applied method is to introduce nanoscale second phases which can provide reinforcement or functionalization purposes. These materials commonly include carbon nanomaterials, rare earth and their oxides, and many hard ceramic nanoparticles [11-15].

Graphene has been extensively explored to enhance functional and mechanical properties of metal matrix nanocomposites for wide-range applications due to its superior mechanical, electrical and thermal properties [16-20]. However, strengthening using graphene in the graphene/Cu system often shows limited effect due to the easy agglomeration of graphene in the matrix and a weak interfacial bonding between graphene and Cu matrix. This weak bonding is mainly due to the large specific surface areas and van der Waals force of graphene, and the poor wettability of carbon materials (e.g., graphene) with metal of Cu (e.g., the contact angle between Cu and graphite is ~140°).

One of the viable approaches to improve dispersion and wettability of graphene inside the metal matrix composites is to coat it with suitable nanomaterials of metals or carbides [17, 21]. These metal or carbide nanoparticles/nanolayers decorated onto the surfaces of carbon nanomaterials can effectively minimize the density differences between graphene and metal matrix, thus leading to improved dispersion effects of graphene. For example, we recently reported that a good balance of strength and ductility was achieved in a Ti composite using reduced graphene oxide nanosheets decorated with metal or ceramics nanoparticles [17, 21]. Chu et al. [22] also improved the interfacial adhesion and tensile strength of reduced graphene oxide /CuCr composites by alloying with Cr to *in-situ* form a nanolayer of Cr_7C_3. We previously also introduced Cu-coated graphene nanoplates (Cu@GNPs) into the CuW composites using electroless plating and spark plasma infiltrating sintering [12]. Results showed that electrical conductivity, thermal conductivity, and micro-hardness have been increased up to ~ 95.3%, ~ 24.3%, and ~ 28%, respectively, compared with those from the conventionally sintered CuW powders. Although the electrical and mechanical properties of CuW composites reinforced with modified graphene have been significantly improved, the arc-erosion behavior of CuW electrical contacts doped with nanostructured Cu@rGO is still unsatisfied. A previous study [5] reported that the arc breakdown position on the surface of CuW alloys occurred mainly on the rich Cu phase and Cu/W interfacial zones, where liquid Cu was sputtered intensely and larger cathode craters were formed, accelerating the centralization arc erosion and cracking along Cu/W interface. Hence, interfacial strengthening is critical for long service life-time of CuW electrical contacts composites.

Herein, copper nanoparticles were firstly decorated onto the reduced graphene oxides nanosheets (named as Cu@rGO for simplification) and then further applied as reinforcements to strengthen Cu/W interfaces for fabrication Cu@rGO/CuW composites. Firstly, nanostructured Cu@rGO can effectively minimize the density differences between graphene and the CuW matrix, thus leading to improved dispersion effects of graphene. Secondly, the *in-situ* formed tungsten carbides can enhance the interfacial bonding strength via reactive wetting on the surfaces. The Cu@rGO nanopowders were fabricated using a one-step chemical co-reduction process, and then incorporated into the CuW matrix to fabricate rGO/CuW composites using a powder metallurgy route. The influences of Cu@rGO nanopowders on the microstructure and arc erosion resistance were investigated. The key mechanisms of rGO/CuW composites arc breakdown were further studied. Tungsten carbides with irregular shapes were *in-situ* formed during sintering process. Results showed that the electrical breakdown strength of 3 wt% Cu@rGO/CuW composites were increased by 28.9% in comparison with those of the CuW composites. The reasons can be attributed to: (a) Addition of nanostructured Cu@rGO increases the viscosity of molten metal Cu, thus inhibiting the significant flow and splashing of molten metal; (b) The lower work functions of carbon and tungsten carbide restrained the electron emission; and (c) Tungsten carbides with their good stability and high melting point shorten the solidification time of molten copper liquid, thus extending service life time of the Cu@rGO/CuW composites.

2. Materials and Experimental methods

2.1 Materials and methods

Graphene oxides nanosheets (GONs) prepared using the Hummers method were purchased from XFNANO Technology Co., Ltd., China. A transmission electron microscope (TEM) image shown in **Figure 1(a)** reveals that the GONs have large-scale, transparent, and folded structures. However, there are many nanoscale defects at the boundary of GONs (inset in **Figure 1a**), which could facilitate the easy *in-situ* deposition of Cu nanoparticles onto the surfaces of GONs. Select electron diffraction pattern of the GONs shown in **Figure 1b** confirms the low degree of crystallinity for the GONs.

The as-synthesized GONs were reduced into the rGOs and simultaneously coated with Cu nanoparticles (Cu@rGO) using an one-step chemical co-reduction route. All the chemicals were used directly without further purification. **Figure 2a** shows the detailed schematic illustrations of the fabrication process of Cu@rGO nanoparticles formed by one-step chemical co-reduction route. Macrophotograph of the fabricated Cu@rGO nanopowders in **Figure 1(c)** shows the color was changed from brown (GO's color) into black after one-step chemical co-reduction method. Scanning electron microscope (SEM) image of as-synthesized Cu@rGO nanopowders in **Figure 1(d)** shows that the Cu nanoparticles (confirmed by EDS analysis in **Figure 1e** and **Figure 1f**) with a spherical one or a hexahedron one are uniformly distributed on the surfaces of wrinkled rGO nanosheets.

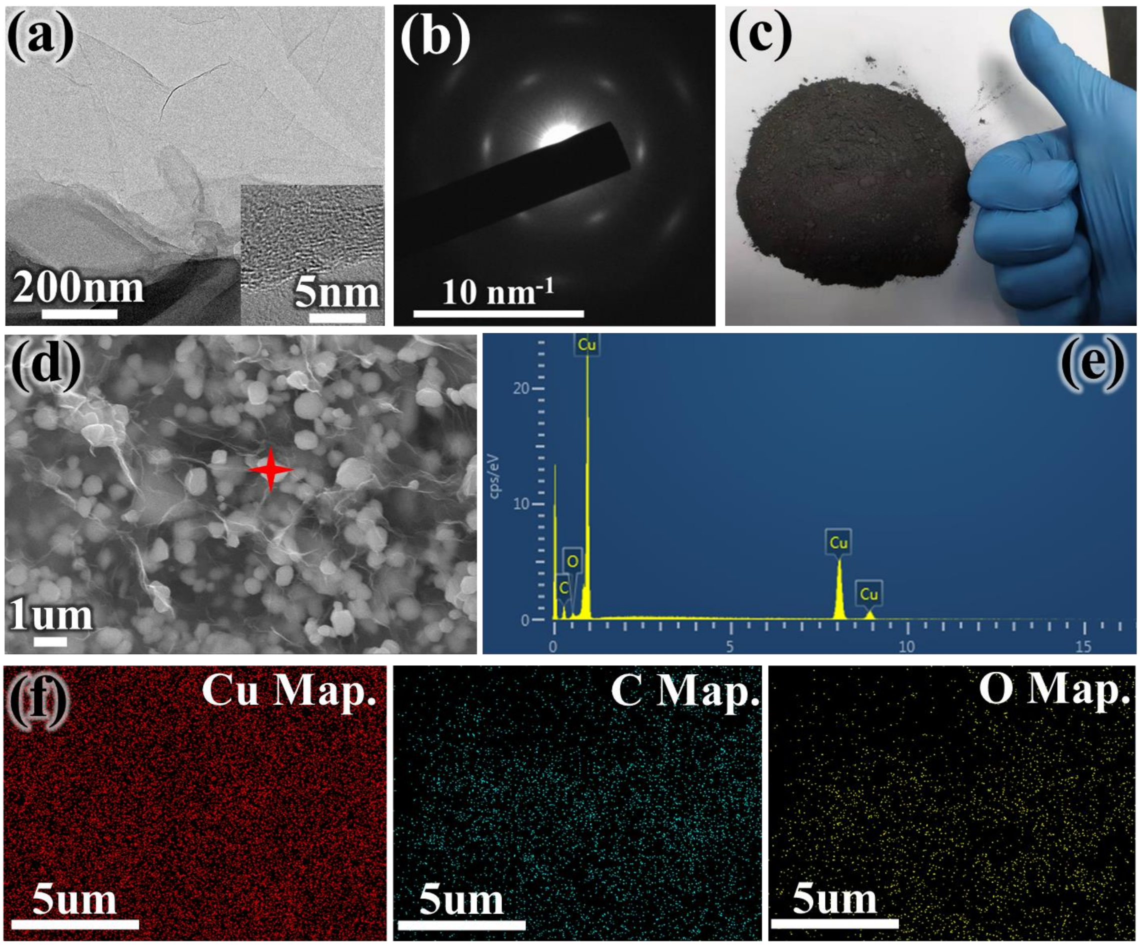

Figure 1(a) TEM image of graphene oxides, inset showing the high resolution TEM of

GO; (b) Selected electron diffraction pattern; (c) Macrophotograph of fabricated Cu@rGO nanopowders; (d) SEM image of Cu@rGO nanocomposites, (e) EDS point analysis of marked region in Figure (d), (f) EDS mapping results of Figure (d), respectively.

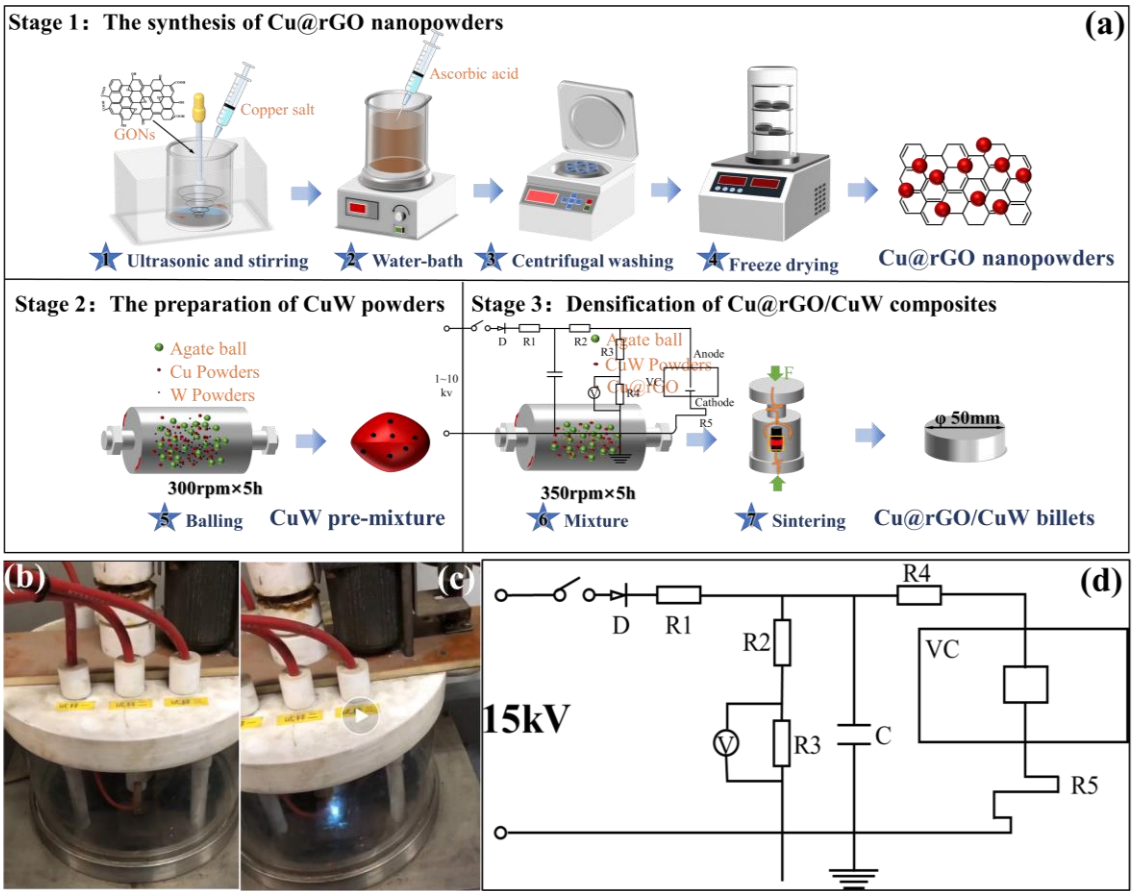

Figure 2(a). Schematic illustration of microstructure of Cu@rGO/CuW composites fabricated using combination of *in-situ* co-reduction method, ball milling and SPS; (b) the state before the breakdown; (c) the momentary state of the breakdown and (d) experimental circuitry diagram of vacuum struck, respectively.

Commercially available tungsten powders (1~2 μm in size, purity of 99.9%) and electrolytic copper powder (4~7 μm in size) were selected to fabricate CuW composites. The copper modified reduced graphene oxides/CuW composites (i.e. Cu@rGO/CuW) were fabricated using combined *in-situ* co-reduction method [23, 24], ball milling and spark plasma sintering (SPS) technology, as shown in **Figure 2**. Mixed powders with 30 wt% copper and 70 wt% tungsten were used as the initial sources, which were firstly blended in a drum ball mill (QM-5) for 5 hrs at a rotating speed of 300 rpm, with a mass ratio of ball and powder of 3:1. During this process, the soft copper powder particles were deformed and the W particles were adhered onto the surfaces of copper particles. Subsequently, the milled CuW mixtures with various Cu@rGO nanopowders were further milled in a drum ball milling machine at 350 rpm for 5 hrs with a ball to powder ratio of 1.5:1. Finally, the Cu@rGO/CuW composite powders were densified using SPS at 1000 ºC for 10 min with an axial pressure of 45 MPa in a vacuum atmosphere. In addition, CuW composites as a control group were fabricated by the same process.

For more detailed microstructural information of the constituting phases in the sintered composites, the 3wt%Cu@rGO/CuW composites was taken as an example for further TEM analysis as shown in **Figure 3**. According to the bright field image shown in **Figure 3a**, no visible gaps or cracks were found in the composite, revealing that a good bonding formed between W and Cu phases. The corresponding selected area diffraction (SAED) patterns shown in **Figure 3a$_1$** and **Figure 3(a$_2$)** confirm the face centred cubic phase of Cu and body-centrered cubic phase of W. However, rGOs with a width of ~100 nm are well embedded and bonded with the Cu matrix without the presence of cracks, as shown in **Figure 3b**. EDS mapping analysis reveals the diffusion reaction between rGO and W matrix during the sintering, as shown in **Figures 3b$_1$** and **3b$_3$**. The formation of tungsten carbides in CuW composites is in favor of improvements of their mechanical and arc erosion resistance [14, 25, 26]. As shown in **Figure 3c**, the microstructure of the CuW composites without adding Cu@rGO is relatively uniform and dense. The gray quasi-spherical phase comprises tungsten particles, which form into a continuous skeleton structure. The black network structure is the copper phase. However, when adding Cu@rGO nanopowders, as shown in **Figure 3d**, the quasi-spherical tungsten particles are changed into angular ones, indicating that the addition of Cu@rGO nanopowders resulted in new tungsten phases. EDS analysis in **Figure 3d** and XRD results in **Figures 3e** and **3f** further confirm the formation of tungsten carbide particles owing to their lower Gibbs free energy.

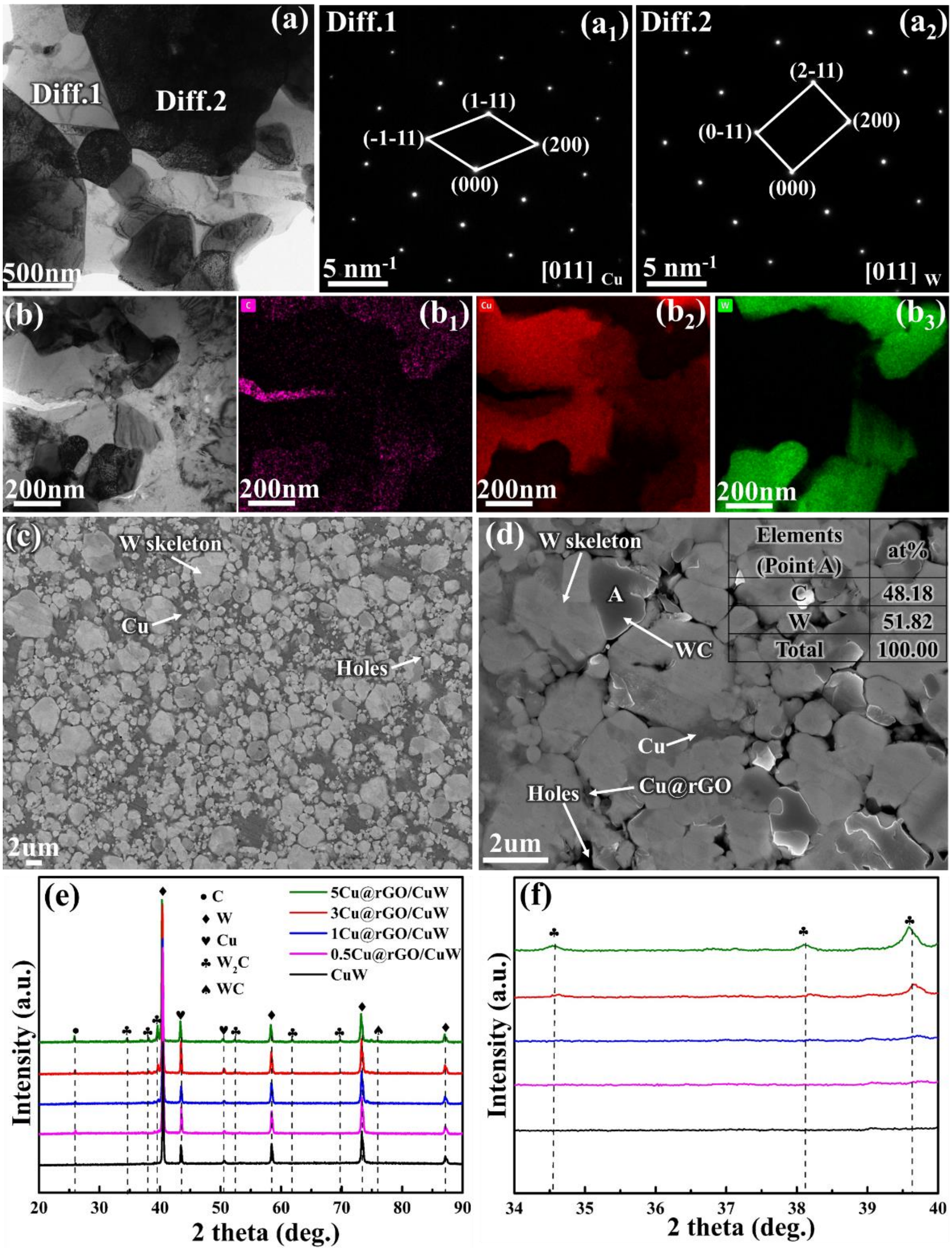

Figure 3. (a) Bright field image of CuW composites; (a_1) and (a_2) SEAD pattern taken from marked region Diff. 1 and Diff. 2 in Figure a; (b) Bright field image of 3wt%Cu@rGO/CuW composites and (b_1) ~ (b_3) corresponding EDS mapping results; SEM images of (c) CuW composites and (d) 3wt% CuW composites; (e) X-ray diffraction analysis results of CuW composites with Cu@rGO nanopowders; (f) enlarged XRD patterns at $2\theta = 34°\sim40°$ in Figure (e), respectively.

2.2 Characterizations

Microstructures of Cu@rGO and Cu@rGO/CuW composites were characterized using a field emission scanning electron microscope (FESEM, Zeiss GeminiSEM 500) and a high-resolution transmission electron microscope (HRTEM, JEOL JEM-2100Plus) with selected area electron diffraction (SAED). For TEM sample preparation, about 0.2 mm flake was obtained using a wire-cutting machine, mechanically ground to a thickness of 30~50 μm using a metallographic sand paper, and was then carried out using a Gatan PIPS 691 ion milling system with a time of 6 hrs and argon ions were used in the ion etching with the accelerating voltage in the range of 2.5–5 keV and with an incident angle in the range of 4–10°. The phase compositions were investigated using X-ray diffraction (XRD) with a Cu Kα radiation.

Schematic illustrations of the testing facility and experimental circuitry diagram of vacuum struck are shown in **Figures 2b** ~ **2d**. A pure W needle with a tip radius of 3 mm was used as an anode. The composite samples were first polished mechanically, and then placed in the vacuum chamber as a cathode. SF_6 gas was used as an arc extinguishing medium when the electrical contact was switched on and off with a voltage of 15 kV. Subsequently, the anode electrode was moved to the surface of the sample at the speed of 0.01 mm/min until the electric breakdown occurred between electrodes. As shown in **Figure 2c**, a strong bright electrical arc was observed at the surface of samples, resulting in the complex physical and chemical reactions during the arc breakdown process. The distance for migration between cathode and anode was measured using a digital micrometer. After the arc extinguished, the electrical breakdown test was repeated 100 times. The breakdown strength was obtained using the breakdown voltage divided by the breakdown gap [27]. The surface morphologies of samples after arc breakdown were determined using the SEM with an energy dispersion spectrometer (EDS). X-ray photoelectron spectroscope (XPS, Thermo Fisher ESCALAB Xi+) was used to examine the chemical states of surface elements after arc breakdown. The 3D morphology of the ablated surface after 100 times arc breakdown was characterized using a three-dimensional profilometer (America, KLA Tencor-MicroXAM-800).

3. Results and discussion

Arc erosion resistance is a key parameter for CuW composites to be used as the electrical contact materials [27]. Relationships between arc breakdown strength and number of break-down of the specimens with various Cu@rGO concentrations were obtained under a voltage of 15 kV. The obtained results shown in **Figure 4** reveal that the dielectric breakdown strength of CuW composites was relatively stable over 100 electrical breakdown cycles, and the average strength was ~ 4.5×10^6 V/m. However, with an increase of the Cu@rGO contents, the average dielectric breakdown strength of the specimens was increased. The calculated average dielectric breakdown strengths of the specimens with 0.5 wt%, 1.0 wt%, 3 wt% and 5.0 wt% Cu@rGO were 4.6×10^6 V/m, 4.8×10^6 V/m, 5.8×10^6 V/m, and 5.5×10^6 V/m, respectively, revealing that the addition of Cu@rGO nanopowders has enhanced the average dielectric strength of CuW composites, which is 28.9% larger than that of CuW matrix.

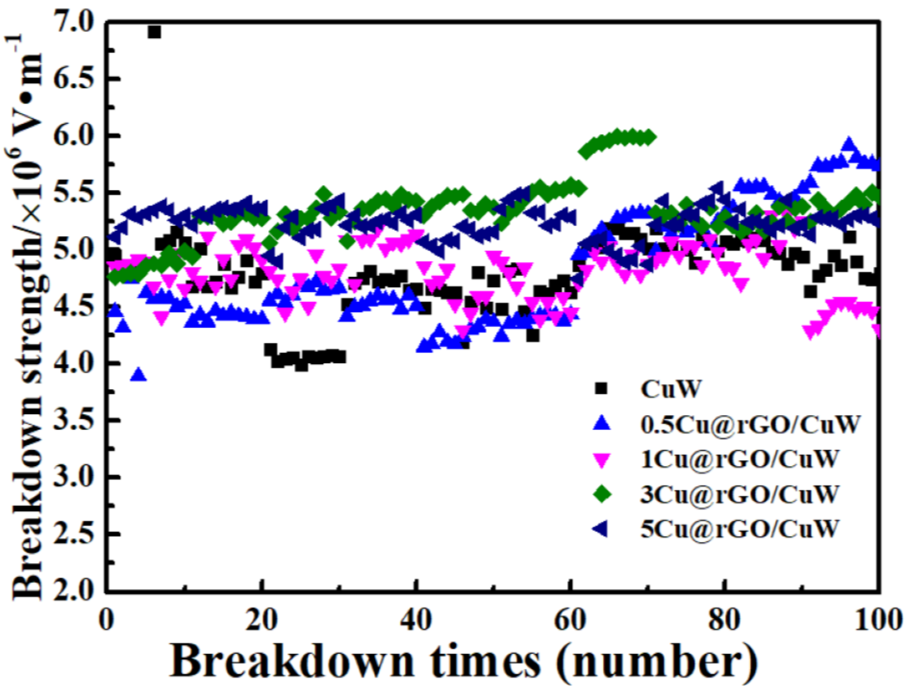

Figure 4. The relationships between electrical breakdown strength and breakdown times of the CuW composites without and with various Cu@rGO nanopowders, respectively.

In order to determine the first breakdown phases and places of arcs, surface morphologies of CuW alloy and Cu@rGO/CuW composites after the first arc breakdown in SF_6 atmosphere were observed using SEM, and the obtained image is shown in **Figure 5**. A circular arc erosion region with 0.0176625 mm^2 can be observed on the surface of CuW alloy. A micro-size hole was observed in the arc erosion region owing to the evaporation of the low melting point Cu phase. The EDS of irregular protrusion (denoted by point A in **Figure 5a**) in **Figure 5(a_1)** reveals the main peaks of Cu and a small quantity of W owing to the condensation of copper vapor. Whereas, the arc erosion craters of Cu@rGO/CuW composites with 0.005024 mm^2 are smaller and shallower than those of CuW composites, as compared **Figures 5a** and **5b**. It can be seen in **Figure 5b** that the breakdown pits on the surface of Cu@rGO/CuW composites are dispersed uniformly, and the protrusion is smaller than that in **Figure 5a**. EDS result of point C (Inset in **Figure 5b**) reveals a dominant carbon main peaks with a small quantity of Cu and W elements, revealing that the graphene was subjected arc breakdown during the first breakdown.

According to the field emission theory [28, 29], under the action of external electric field, interface atoms and electrons are easy to escape due to the weaker binding force which comes from the CuW bonding interface. Besides, the occurrence of breakdown is closely related to the work functions of metal elements under the same electrical breakdown conditions, and Cu phase has a lower work function. Therefore, discontinues electrical breakdowns of CuW composites usually occurs on the Cu/W phase interfaces and copper-rich regions, and the arc cannot be moved rapidly on the surface of CuW alloy as shown in **Figure 5a**. Whereas, when the Cu@rGO nanopowders was introduced into CuW matrix, the interfaces of Cu/W phase were strengthened owing to the diffusion of carbon atom and formation of tungsten carbide particles in the composites, which makes the Cu/W interface forming a strong metallurgical bonding. As a result, the Cu/W interfacial energy is decreased because the element of C is dissolved and diffused into W phase at the interface [30].

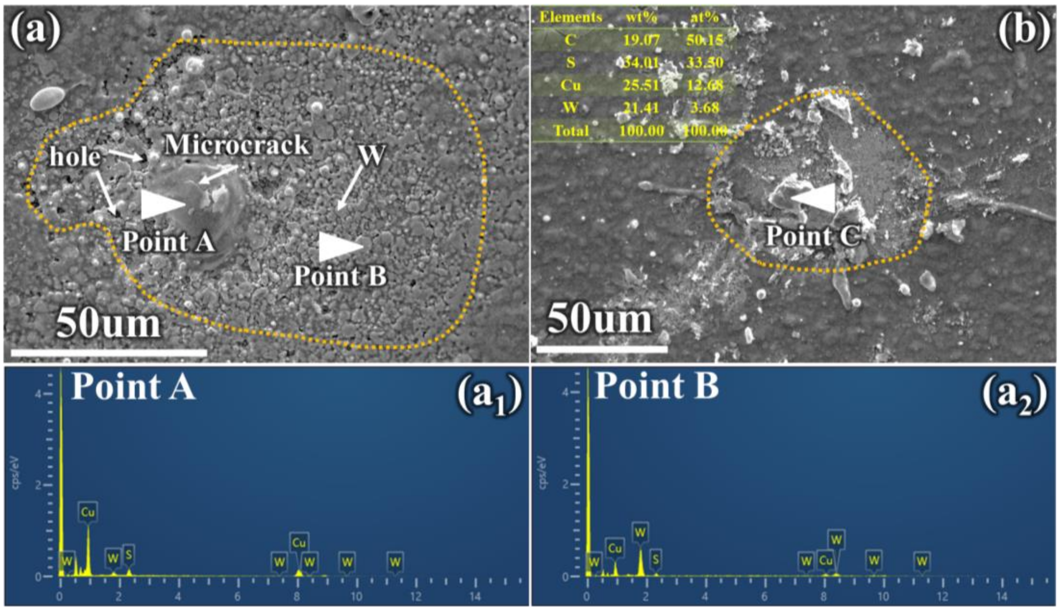

Figure 5. SEM images of CuW and Cu@rGO/CuW composites after the first electrical breakdown (a) CuW composites, (a_1) and (a_2) EDS analysis of point A and point B marked in Figure (a), (b) Cu@rGO/CuW composites, inset showing the EDS result of point C in Figure (b), respectively.

SEM micrographs of sample surfaces with different contents of Cu@rGO nanopowders after 100 breakdown cycles are presented in **Figure 6**. It can be seen from **Figures 6(a)~(a_1)** that the most serious arc erosion with rough morphology occurred in the central region just underneath the tungsten anode tip. EDS mapping analysis in **Figure 6(a_2)** shows that the droplets and their surrounding areas have mainly the elements of F, S, Cu and W. The F and S elements are from the protective atmosphere of SF_6 in the working environment of the electrical contact, indicating SF_6 extinguish medium has been involved in surface chemical reactions under the high temperature arc process [23], which eventually causes the CuW contacts to lose their functions of conducting in the course of long-term service. Whereas, with an increase in the

Cu@rGO contents, the breakdown pits were decreased in depth and became increasingly diffused, as compared with **Figures 6(b)** ~ **(e)**. The above results indicate that the ability of the specimens to disperse arc became dramatically enhanced owing to the presence of Cu@rGO.

XPS analysis of the Cu@rGO/CuW composites after breakdown for 100 cycles in **Figure 7** shows the presences of the C1s and Cu $2p^3$ peak, further revealing the graphene was reserved after the electrical breakdown. Moreover, the 3D profiles analysis in **Figure 6(f~j)** reveals that addition of Cu@rGO nanopowders can significantly reduce the roughness of samples after arc ablation. This is mainly due to the following reasons. (a) The ceramic particles are generated by the reaction between the tungsten skeleton and rGO during the high temperature sintering process (**Figures 3d** ~ **f**); (2) The superior thermal conductivity of graphene improves the wetting capabilities of matrix during the arc breakdowns process, (3) Cu@rGO nanophases have a lower working function compared with those of W and Cu phases [20], and (4) There is an enhanced W/Cu interfacial bonding owing to diffusion and *in-situ* reactions (**Figure 3b**).

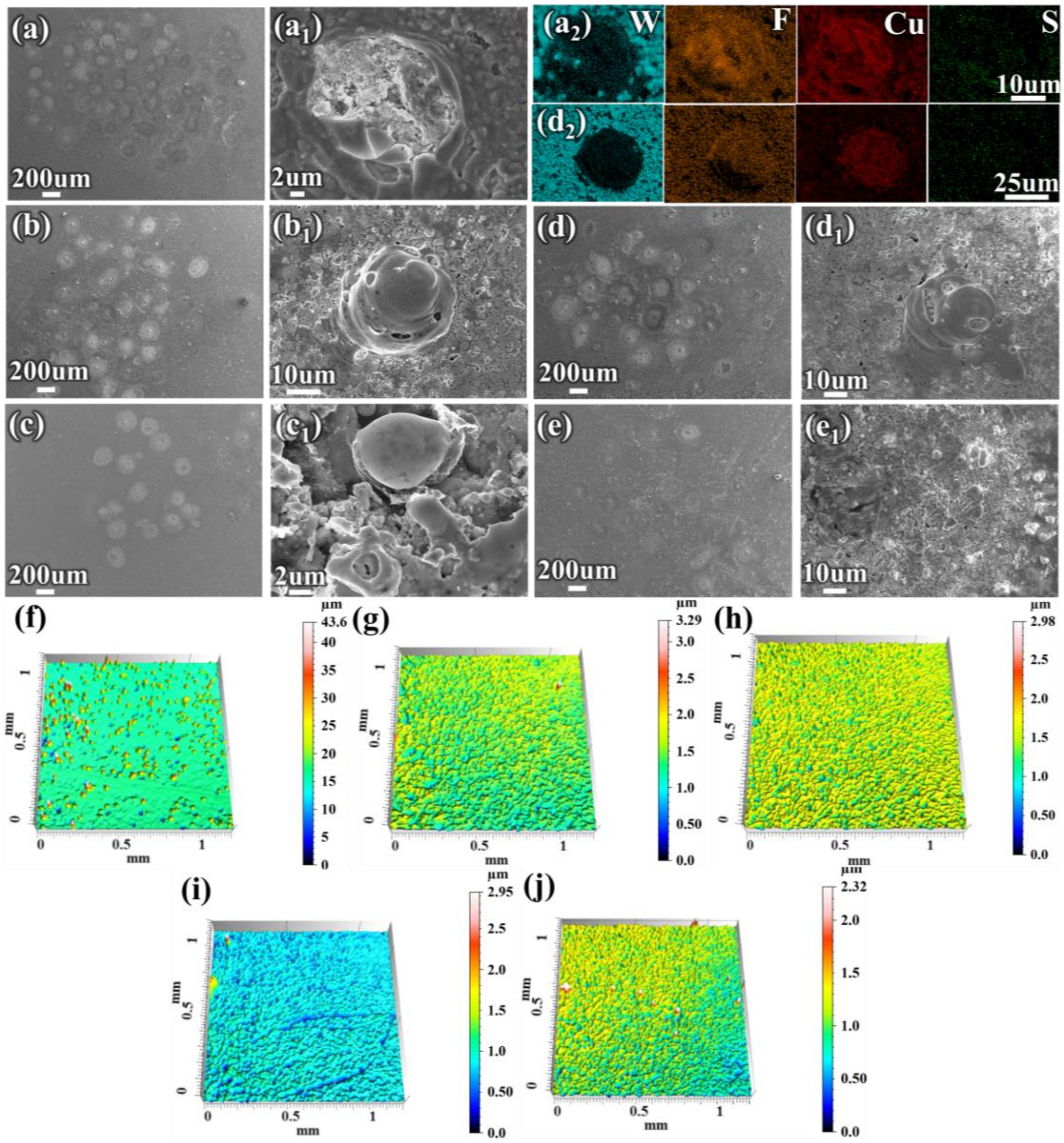

Figure 6. SEM image of **s**urface morphologies and corresponding 3D profiles after electrical breakdown for 100 cycles of CuW composites with different contents of Cu@rGO (a, f) 0 wt%, (b, g) 0.5 wt%, (c, h) 1 wt%, (d, i) 3wt% and (e, j) 5wt%, respectively.

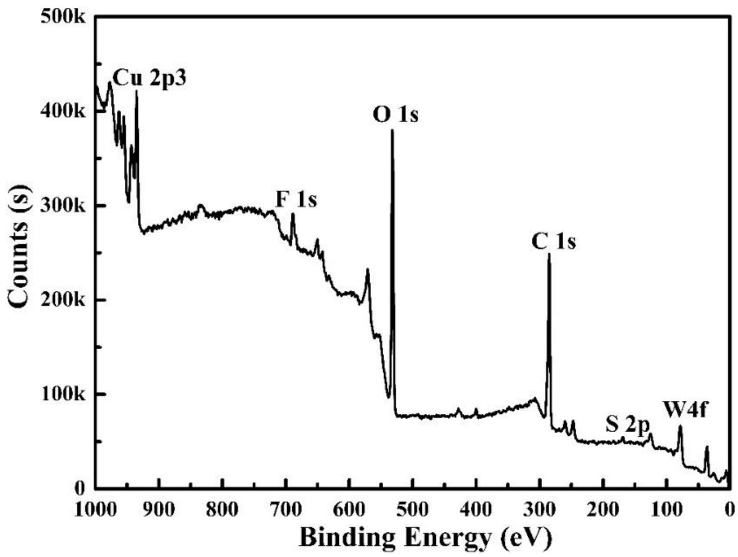

Figure 7. XPS survey spectrum of the Cu@rGO/CuW composites after electrical breakdown for 100 cycles.

For the CuW system, the melting point of Cu is much lower than that of W, therefore, the Cu phases around the W skeleton structures are melt and evaporated to the contact surface during the arc-erosion process as shown in **Figure 5a**. With the increased breakdown time, the W skeleton structure is constantly peeled off (**Figure 8b$_4$**). After arc extinguished, obvious ablation pits are formed on the sufrace of CuW composites (**Figure 8a$_6$**). Therefore, as reported in references [5, 29, 31, 32], the main mechanisms of ablation failure for the CuW contact materials are splashing and evaporation of the Cu phases, and ablation of the W skeleton (**Figure 5a** and **Figure 8a**).

There are many factors that may affect the arc ablation proprties of electrical contact materials, such as the roughness of contact surface, the shape and size of the contact materials and the external magnetic field [23]. However, the most important ones are determined by the physical properties of the contact material itself, such as its work function, electron potential barrier and microstructure characteristics. For the Cu@rGO/CuW composites as shown in **Figures 8b ~ b_7**, when the Cu molten pool is firstly produced under the effect of high arc energy, Cu@rGO will increase the viscosity of the molten metal Cu owing to Cu@rGO's low density, so it will float on the surface of molten metal Cu (**Figure 8b_1 ~ b_2**). This can stabilize the molten pool, thus inhibiting the flow and splashing of molten metal to reduce arc ablation.

Furthrmore, Cu nanoparticles are not completely coated on the surface of reduced graphene oxides nanosheets (**Figure 1d**), the C atoms (derived from rGO) can be *in-situ* formed from W skeleton during the SPS owing to low Gibbs free energy of tungsten carbide. According to the work function theory, the arc would occur firstly on the phase with a smaller work function during dielectric breakdown process. The work functions of tungsten, copper, graphene and tungsten carbide are 4.54 eV [14], 4.36 eV [14], 4.2 eV [33] and 3.79 eV [14], respectively. Therefore, breakdowns may preferentially occur on the tungsten carbide phase and Cu@rGO phase instead of Cu phase, thus slowing down the spatter of copper. When the arc breakdown occurs, graphene cladding can restrain the electron emission, causing the efficeint transfer of heat generated by the arc.

Besides, under the heat effect of arc, the tungsten carbides with a good stability at a high temperature are distributed in the CuW matrix, and prevent the flow or the accumulation of molten copper, and also avoid the large area splash of copper liquid. On the other hand, the tungsten carbide ceramic particles with high melting points can be used as the cores of heterogeneous crystal nucleation, which shortens the solidification time of molten copper liquid and reduces the size of particles formed on the composite surface (**Figure 8b₆**). Both the above-mentioned factors would contribute to the improved anti-ablation properties and extended service life of Cu@rGO/CuW composites (**Figure 8b₇**).

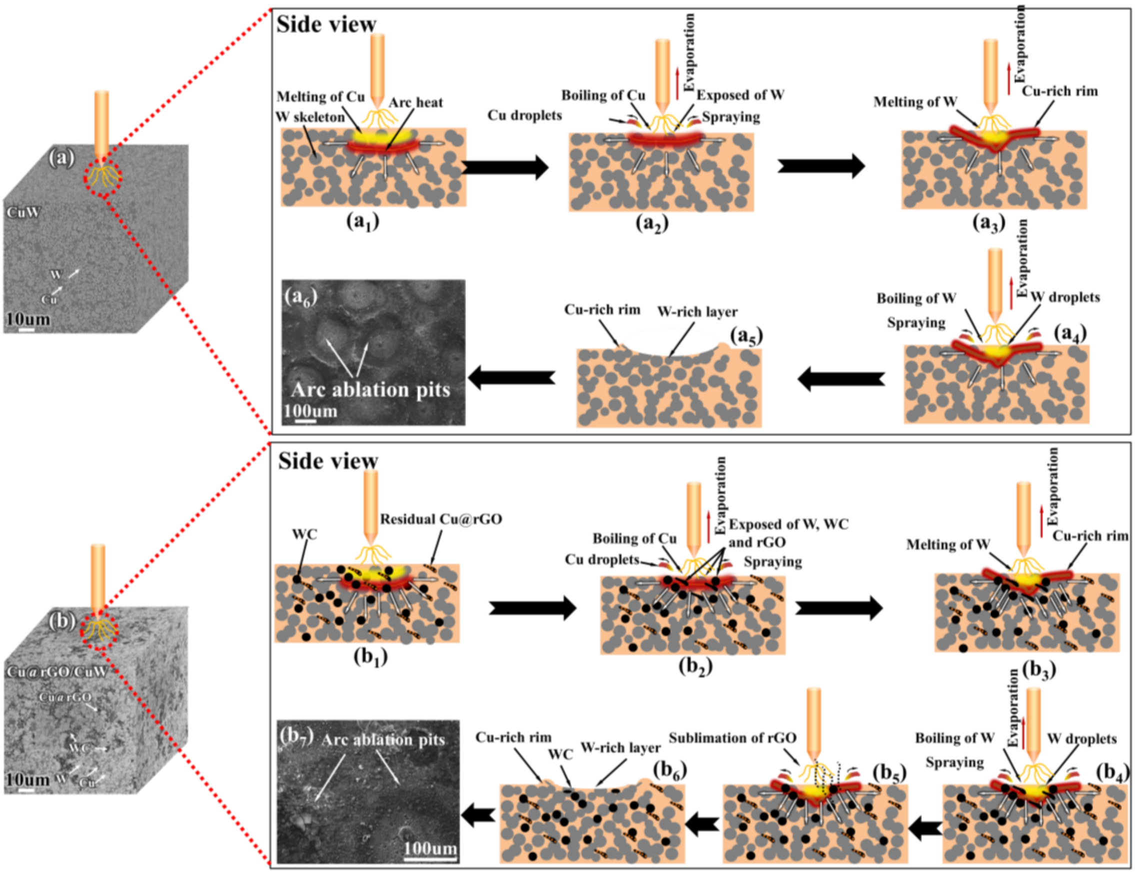

Figure 8. Schematics illustration of the ablation mechanisms of (a~a_6) CuW composites [29] and (b~b_7) Cu@rGO/CuW composites, respectively.

4. Conclusions

In summary, a one-step and co-reduction chemical process strategy was developed to directly modify reduced graphene oxides with Cu nanoparticles for preparing high-performance CuW composites. Tungsten carbide phases were formed through the *in-situ* reaction of rGO and tungsten during the SPS process. The CuW composites with

Cu@rGO showed significantly improved arc erosion resistance. Compared with CuW composites, the ablation area of Cu@rGO/CuW composites was smaller and the ablation craters were shallower, and the average dielectric vacuum breakdown strength of the CuW composites with 3 wt% Cu@rGO was increased by 28.9% in comparison with the CuW composites without Cu@rGO. The arc breakdown mechanism of Cu@rGO/CuW composites are summarized as following. (1) Addition of Cu@rGO increases the viscosity of molten metal Cu, inhibiting the flow and splashing of molten metal; (2) Lower work functions of carbon (i.e. rGO) and tungsten carbide restrains the electron emission; and (3) Tungsten carbides with their good stability and high melting point shorten the solidification time of molten copper liquid, thus extending service life time of Cu@rGO/CuW composites.

Declaration of Competing Interest

The authors declare that they have no known competing financial interests or personal relationships that could have appeared to influence the work reported in this paper.

Acknowledgments

The authors would like to acknowledge the financial support from National Natural Science Foundation of China (No. 51901192), the Shaanxi Science Foundation For Distinguished Young Scholars (2020JC-50), Key Research and Development Projects of Shaanxi Province (No. 2019GY-164), Foundation of Northwest Institute for

Non-ferrous Metal Research (No. YK2020-9), as well as International Exchange Grant (IEC/NSFC/201078) through Royal Society and National Science Foundation of China (NSFC). We thank Master Hang Xue and Ning Tian at Xi'an Rare Metal Materials Institute Co., Ltd for assistance in carrying out arc ablation experiment, and Professor Wenge Chen at Xi'an University of Technology for the usage of arc ablation equipment.

References

[1] L.L. Dong, M. Ahangarkani, W.G. Chen, Y.S. Zhang, Recent progress in development of tungsten-copper composites: Fabrication, modification and applications, Int. J. Refract. Met. H. Mater. 75 (2018) 30–42.

[2] A.Q. Chen, W.T. Huo, L.L. Dong, W.G. Chen, Y. Zhou, Recent advance of copper tungsten composite materials, Materials China 40(2) (2021) 152-160.

[3] W.G. Chen, L.L. Dong, Z.J. Zhang, H.M. Gao. Investigation and analysis of arc ablation on WCu electrical contact materials, J. Mater. Sci: Mater. Electron. 27(2016) 5584–5591.

[4] V. N. Kolokoltsev, I. V. Borovitskaya, L. I. Ivanov, V. Ya. Nikulin, M. M. Lyakhovitskii, V. V. Paramonova. The structure and current–voltage characteristics of copper–tungsten electric contacts prepared using a plasma focus installation, Inorganic Materials: Applied Research 2(2) (2011) 167–171.

[5] X.H. Yang, J.T. Zou, P. Xiao, X.H. Wang, Effects of Zr addition on properties and vacuum arc characteristics of Cu-W alloy, Vacuum 106 (2014) 16-20.

[6] D.G. Kim, G.S. Kim, M.J. Suk, S.T. Oh, Y.D. Kim, Effect of heating rate on microstructural homogeneity of sintered W-15 wt% Cu nanocomposite fabricated from W-CuO powder mixture, Scr. Mater. 51 (2004) 677-681.

[7] S.N. Alam, Synthesis and characterization of W-Cu nanocomposites developed by mechanical alloying, Mater. Sci. Eng. A 433 (2006) 161-168.

[8] W.G. Chen, P. Feng, L.L. Dong, B. Liu, S.X. Ren, Y.Q. Fu, Experimental and theoretical analysis of microstructural evolution and deformation behaviors of CuW composites during equal channel angular pressing, Mater. Des. 142 (2018) 166–176.

[9] L.C. Zhuo, Y.H. Zhang, Z. Zhao, B. Luo, Q.Y. Chen, S.H. Liang, Preparation and properties of ultrafine-grained W-Cu composites reinforced with tungsten fibers, Mater. Lett. 243 (2019) 26–29.

[10] L.C. Zhuo, Z. Zhao, Z.C. Qin, Q.Y. Chen, S.H. Liang, X. Yang, F. Wang. Enhanced mechanical and arc erosion resistant properties by homogenously precipitated nanocrystalline FCC-Nb in the

hierarchical W-Nb-Cu composite, Compos. Part B 161 (2019) 336–343.

[11] L.L. Dong, W.G. Chen, C.H. Zheng, N. Deng Microstructure and properties characterization of tungsten-copper composite materials doped with graphene, J. Alloy. Compd. 695 (2017) 1637-1646.

[12] W.G. Chen, L.L. Dong, J.J. Wang, Y. Zuo, S.X. Ren, Y.Q. Fu. Synergistic enhancing effect for mechanical and electrical properties of tungsten copper composites using spark plasma infiltrating sintering of copper-coated graphene, Sci. Rep.-UK (2017) 7:17836

[13] L.C. Zhuo, Q.Q. Zhang, Y.H. Zhang, Z. Zhao, S.H. Liang, Q.Y. Chen, H.L. Wang, J.L. Zhang. Tailoring the microstructure and properties of tungsten-copper composites by minor addition of SiC particles for nuclear fusion reactor application, J. Nucl. Mater. 538(2020) 152220

[14] Q. Zhang, Y. Cheng, B.J. Chen, S.H. Liang, L.C. Zhuo. Microstructure and properties of W-25 wt% Cu composites reinforced with tungsten carbide produced by an *in situ* reaction, Vacuum 177 (2020) 109423

[15] Z.L. Liu, L.M. Luo, J.B. Chen, X.M. Huang, J.G. Cheng, Y.C. Wu. Fabrication of W–Cu/CeO_2 composites with excellent electric conductivity and high strength prepared from copper-coated tungsten and Ceria powders, Mat. Sci. Eng. A 626(2015) 61-66.

[16] L.X. Wei, X.Y. Liu, Y.Z. Gao, X.W. Lv, N. Hu, M. Chen. Synergistic strengthening effect of titanium matrix composites reinforced by graphene oxide and carbon nanotubes, Mater. Des. 197 (2021) 109261

[17] L.L. Dong, W. Zhang, Y.Q. Fu, J.W. Lu, X.T. Liu, N. Tian, Y.S. Zhang, Reduced graphene oxide nanosheets decorated with copper and silver nanoparticles for achieving superior strength and ductility in titanium composites, ACS Appl. Mater. Interfaces 2021, 13, 43197−43208

[18] N. Tian, L.L. Dong, H.L. Wang, Y.Q. Fu, W.T. Huo, Y. Liu, J.S. Yu, Y.S. Zhang. Microstructure and tribological properties of titanium matrix nanocomposites through powder metallurgy using graphene oxide nanosheets enhanced copper powders and spark plasma sintering, J. Alloy. Compd. 867 (2021) 159093

[19] L.L. Dong, Y.Q. Fu, Y. Liu, J.W. Lu, W. Zhang, W.T. Huo, L.H. Jin, Y.S. Zhang, Interface engineering of graphene/copper matrix composites decorated with tungsten carbide for enhanced physico-mechanical properties, Carbon 173 (2021) 41-53

[20] D. Dai, M.L. Wu, S.C. Shu, K. Yang, C.T. Lin, Y. Han, Z.X. Zhu, Y. Ding, Y.Z. Song, N. Jiang, Thermal CVD growth of graphene on copper particles targeting tungsten copper composites with superior wear and arc ablation resistance properties, Diam. Relat. Mater. 104 (2020) 107765

[21] H. Xue, M. Zhu, L.L. Dong, W. Zhang, X.C. Sun, Y.M. Wang, Y.Q. Fu, Y.S. Zhang, *In-situ* synthesis of reduced graphene oxide/aluminium oxide nanopowders for reinforcing Ti-6Al-4V composites, J. Alloy. Compd. 905 (2022) 164198

[22] K. Chu, F. Wang, Y.B. Li, X.H. Wang, D.J. Huang, H. Zhang, Interface structure and strengthening behavior of graphene/CuCr composites, Carbon 133 (2018) 127-139

[23] Y.L. Xue, W.G. Chen, J.J. Wang, L.L. Dong, Q. Zhao, Y.Q. Fu. Formation mechanism and cohesive energy analysis of metal-coated graphene nanocomposites using *in-situ* co-reduction method, Materials 2018, 11, 2071.

[24] L.L. Dong, Y.C. Ding, W.T. Huo, W. Zhang, J.W. Lu, L.H. Jin, Y.Q. Zhao, G.H. Wu, Y.S. Zhang. A green and facile synthesis for rGO/Ag nanocomposites using one-step chemical co-reduction route at ambient temperature and combined first principles theoretical analyze, Ultrason. Sonochem. 53 (2019) 152–163.

[25] L.L. Dong, W.T. Huo, M. Ahangarkani, B. Zhang, Y.Q. Zhao, Y.S. Zhang, Microstructural evaluation and mechanical properties of *in-situ* WC/W-Cu composites fabricated by rGO/W-Cu spark plasma sintering reaction, Mater. Des. 160 (2018) 1196–1207.

[26] Q. Zhang, S.H. Liang, L.C. Zhuo, Fabrication and properties of the W-30wt%Cu gradient composite with W@WC core-shell structure, J. Alloy. Compd. 708 (2017) 796-803.

[27] Y.X. Zhou, Y.L. Xue, K. Zhou, Failure analysis of arc ablated tungsten-copper electrical contacts, Vacuum 164 (2019) 390–395

[28] J.M. Lafferty, Foundation of vacuum science and technology, John Wiley & Sons Inc, USA, 1998, 20-26.

[29] X. Wei, D.M. Yu, Z.B. Sun, Z.M. Yang, X.P. Song, B.J. Ding, Arc characteristics and microstructure evolution of W-Cu contacts during the vacuum breakdown, Vacuum 107 (2014) 83-89.

[30] Y.R. Li, C. Hou, H. Lu, S.H. Liang, X.Y. Song, WC strengthened W–Cu nanocomposite powder synthesized by in-situ reactions, Int. J. Refract. Met. H. Mater. 79 (2019) 154-157.

[31] M. Ahangarkani, K. Zangeneh-Madar, S. Borji, Z. Valefi, Microstructural study on ultra-high temperature erosion mechanism of infiltrated W-10wt%Cu composite, Int. J. Refract. Met. H. Mater. 67 (2017) 115-124.

[32] W.G. Chen, M.Z. Chen, L.Q. Xing, J.S. Li, F. Hong, Effect of doping on electrical arc characteristic of WCu electrical contact materials, T. Nonferr. Metal. Soc. 19(11) (2009) 2029-2037.

[33] L.L. Dong, W.G. Chen, N. Deng, J.L. Song, J.J. Wang, Investigation on arc erosion behaviors and mechanism of W70Cu30 electrical contact materials adding graphene, J. Alloy. Compd. 696 (2017) 923-930.